JOURNAL OF THE ROYAL SOCIETY Interface

J. R. Soc. Interface (2008) **5**, 285–296
doi:10.1098/rsif.2007.1124
Published online 11 July 2007

Extremely fast prey capture in pipefish is powered by elastic recoil

Sam Van Wassenbergh[1,*], James A. Strother[2], Brooke E. Flammang[3,4], Lara A. Ferry-Graham[4] and Peter Aerts[1,5]

[1]*Department of Biologie, Laboratory for Functional Morphology, University of Antwerpen, Universiteitsplein 1, 2610 Antwerpen, Belgium*
[2]*Ecology and Evolutionary Biology, University of California, 321 Steinhaus Hall, Irvine, CA 92697-2525, USA*
[3]*Museum of Comparative Zoology, Harvard University, 26 Oxford Street, Cambridge, MA 02138, USA*
[4]*Moss Landing Marine Laboratories, 8272 Moss Landing Road, Moss Landing, CA 95039, USA*
[5]*Department of Movement and Sports Sciences, Ghent University, Watersportlaan 2, 9000 Gent, Belgium*

The exceptionally high speed at which syngnathid fishes are able to rotate their snout towards prey and capture it by suction is potentially caused by a catapult mechanism in which the energy previously stored in deformed elastic elements is suddenly released. According to this hypothesis, tension is built up in tendons of the post-cranial muscles before prey capture is initiated. Next, an abrupt elastic recoil generates high-speed dorsal rotation of the head and snout, rapidly bringing the mouth close to the prey, thus enabling the pipefish to be close enough to engulf the prey by suction. However, no experimental evidence exists for such a mechanism of mechanical power amplification during feeding in these fishes. To test this hypothesis, inverse dynamical modelling based upon kinematic data from high-speed videos of prey capture in bay pipefish *Syngnathus leptorhynchus*, as well as electromyography of the muscle responsible for head rotation (the epaxial muscle) was performed. The remarkably high instantaneous muscle-mass-specific power requirement calculated for the initial phase of head rotation (up to 5795 W kg^{-1}), as well as the early onset times of epaxial muscle activity (often observed more than 300 ms before the first externally discernible prey capture motion), support the elastic power enhancement hypothesis.

Keywords: feeding; Syngnathidae; electromyography; energy storage; elasticity; power amplification

1. INTRODUCTION

Based on the force–velocity relationship, the power output of skeletal muscle fibres is intrinsically limited (Hill 1938). In general, we expect force to be proportional to muscle cross-sectional area and velocity proportional to muscle length (i.e. the number of sarcomeres in series), such that power (force×velocity) is theoretically proportional to the volume or mass of the muscle. Therefore, animals may increase power output by increasing muscle mass through training, or over evolutionary time scales. The consequences thereof are particularly important for animals that must achieve a high speed in a short amount of time (Vogel 2005)—acceleration depends on the force produced by muscles, which will only be a fraction of the muscle's maximal isometric force as soon as the muscle fibres start shortening (due to Hill's force–velocity relationship). Consequently, power limits the performance of explosive movement such as jumping (e.g. Marsh & John-Alder 1994), throwing (Stone *et al.* 2003) and escape responses (Wakeling & Johnston 1998; Curtin *et al.* 2005).

However, animals often evade limitations on muscular performance by using power amplification mechanisms to reach higher accelerations. Power (P) can be amplified by storing energy ($E = \int P\,\mathrm{d}t$) in elastic materials, and afterwards releasing this energy in a shorter time (since $P = \mathrm{d}E/\mathrm{d}t$). The force produced during recoil of elastic proteins such as collagen or resilin is a function of the elongation of the elastic structure (e.g. Hooke's Law), and is not subject to a force–velocity relationship. As a result, the quick release of elastic energy amplifies the power available in the muscles that previously caused the elastic deformation, and can thus be a vital tool to enhance performance of explosive movements.

*Author for correspondence (sam.vanwassen bergh@ua.ac.be).

Received 31 May 2007
Accepted 22 June 2007

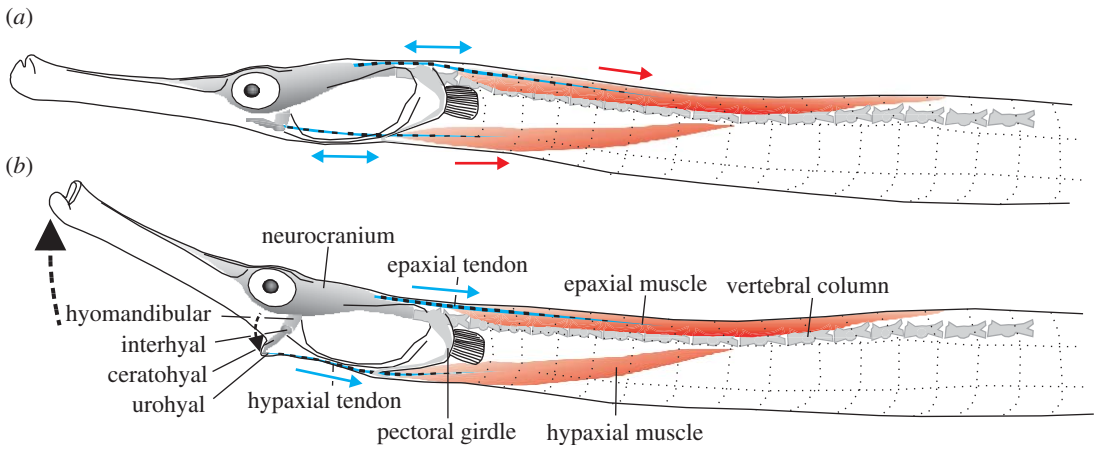

Figure 1. Schematic drawing of *S. leptorhynchus* based on dissections, indicating the most important elements involved in the mechanism of power amplification in Syngnathidae as proposed by Muller (1987). Note that the two major muscles, the epaxials and hypaxials (red), connect to the feeding apparatus by large tendons (blue). Both muscles, as well as the epaxial tendons are left–right paired. The left and right hypaxial tendons, on which the small sternohyoideus muscles also insert (not shown in the figure), converge and become attached posterior of the urohyal (see also Branch 1966). The epaxial tendon continues between the muscle fibres and could be distinguished until beyond the middle of the muscle. Moving posteriorly into the epaxial muscle, the fibres gradually show a decreasing angle of pennation with respect to the central tendon. Manipulation of specimens showed that the pectoral girdle could not be rotated with respect to the vertebral column. According to the hypothesis by Muller (1987), tension is loaded in the tendons prior to prey capture (*a*) during which the configuration of the hyoid (ceratohyal, interhyal) prevents neurocranial elevation. At this time, the clockwise torque on the neurocranium resulting from the forces pulling the epaxial tendons is balanced by a counterclockwise torque exerted by the hypaxial tendon via the hyoid on the neurocranium (onto which rotation of the hyomandibular is highly constrained in the sagittal plane). In this elevated and adducted position, the hyoid may be stabilized by fitting into a groove of the hyomandibula (de Lussanet & Muller 2007). Once the hyoid is 'unlocked' from this position (*b*), recoil of the tendons would cause the neurocranium and the hyoid to accelerate extremely quickly.

Like certain types of locomotion, such as jumping or escape initiations, prey capture can benefit from power amplification, as fast acceleration is critical for predators feeding on elusive prey. Indeed, in order to minimize the chance of prey escape, the predator–prey distance should be decreased as quickly as possible. Well-known examples of elastic energy storage and release to amplify power during feeding in vertebrates are the tongue-projection mechanisms in chameleons (Herrel *et al.* 2000; De Groot & Van Leeuwen 2004), salamanders (Deban *et al.* 2007) and toads (Lappin *et al.* 2006).

It is hypothesized that fishes of the family Syngnathidae (e.g. pipefish, sea horses, sea dragons) also posses a mechanism to amplify power during feeding (Muller 1987). Prey capture in these fishes is initiated by a sudden rotation of the head, bringing the mouth to the prey within a few milliseconds (Muller 1987; Bergert & Wainwright 1997; de Lussanet & Muller 2007). Next, the mouth cavity is expanded, causing the prey to be sucked through the long snout (de Lussanet & Muller 2007). The extremely short duration (6 ms or less; Bergert & Wainwright 1997; Colson *et al.* 1998; de Lussanet & Muller 2007) of syngnathid prey capture is suggestive of possible power amplification. Muller (1987) identified a mechanism by which these fishes can bring their feeding apparatus into a 'locked' position—dorsal rotation of the head will be obstructed when the hyoid is fully elevated (figure 1*a*; ceratohyal and tendon are in line). This would allow the large, post-cranial muscles (epaxials and hypaxials) to be activated without causing any head rotation or hyoid movement (figure 1*a*). A small deviation from this locked position of the hyoid, initiated by a trigger muscle (potentially by activation of the *m. protractor hyoidei* or by relaxation of the *m. add. arcus palatini*), would cause an explosive suction event driven by elastic recoil of the tendons of the epaxial and hypaxial muscles (Muller 1987, 1989; figure 1*b*).

In this study, we tested whether power amplification by elastic energy storage and release is used by the bay pipefish (*Syngnathus leptorhynchus*) during prey capture. To do so, two different approaches were used. Firstly, an inverse dynamic model was developed to calculate instantaneous power requirement of head rotation. Kinematic data quantified from high-speed videos of pipefish performing prey capture served as input to the model. If the calculated power requirement exceeds the maximal power that theoretically can be produced by active contraction of muscle, this would indicate the use of a power amplification system. Secondly, electromyography (EMG) of the epaxial muscles, which power head rotation, was performed in order to test whether epaxial activation precedes head motion, thereby enabling elongation of the tendons prior to prey capture. Such elongation would be essential for generating the stored energy necessary for power amplification.

2. MATERIAL AND METHODS

2.1. High-speed video

Two bay pipefish (*S. leptorhynchus*) were used in experiments during which high-speed video and EMG (see further) were recorded simultaneously. These animals were caught at Friday Harbor, San Juan Islands, USA. The cranial lengths were 20.49 and

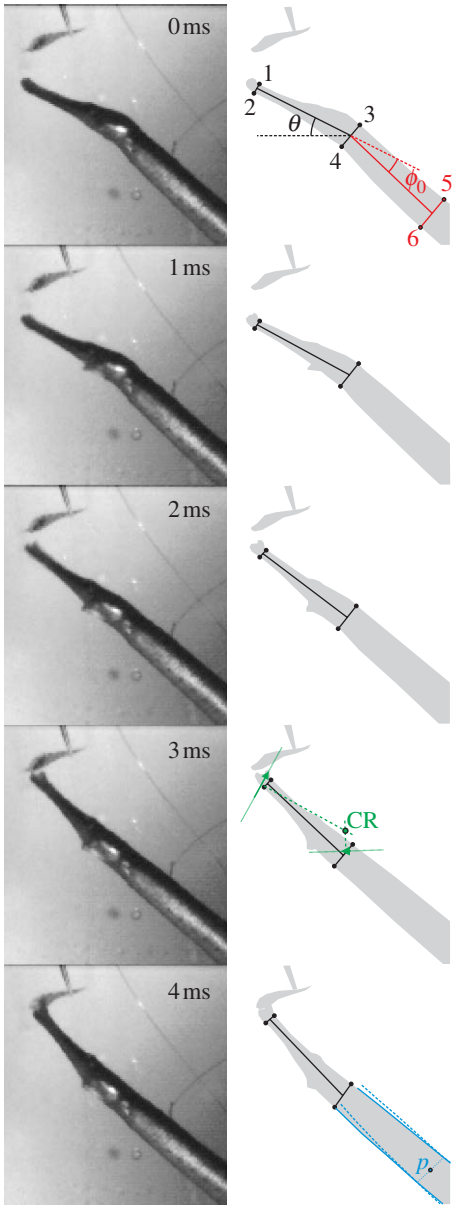

Figure 2. Prey capture sequence of *S. leptorhynchus* feeding on a mysid shrimp held by forceps. The measured kinematic variables are illustrated on the right: the head angle (θ; black), head to body angle at $t=0$ ms (ϕ_0; red). These angles were calculated based on six landmarks on the pipefish as indicated on the top drawing (1–2, anterior tip of the snout; 3–4, posterior region of the head at the level of the opercular opening; 5–6, approximately one head length further down the body). The determination of the centre of rotation (CR, green) based on the displacement of the upper jaw tip and the dorsal edge of the operculum between $t=0$ and 3 ms is illustrated in the drawing of $t=3$ ms. Point p (blue) is the mid-sagittal landmark on the pipefish's body where the ventral movement by the body during dorsal head rotation is approximately negligible. This point was determined from dorsal and ventral body contour tracings of the first frame ($t=0$ ms) and the frame at $t=4$ ms of the high-speed video by taking the xy-average of the points on the body where the corresponding contour lines have converged.

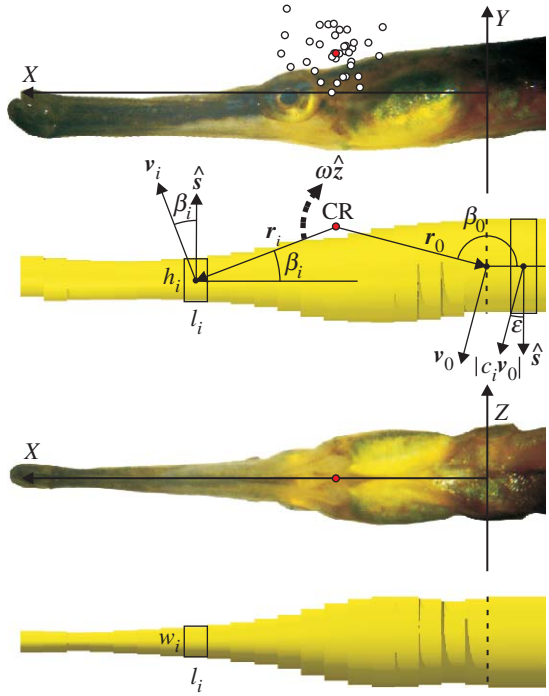

Figure 3. Geometry and symbols of the model used for calculating power requirement during prey capture in pipefish. Open circles on the top picture are the centres of rotation for each of the analysed feeding sequences. The average of these points will be referred to as the CR (centre of rotation, red circle). The following reference frame was used: the line through the middle between the right and left posteriormost points on the opercula was defined as the Z-axis. The origin (0,0,0) is the middle between these two points. The X-axis runs to the dorsal tip of the snout (i.e. the base of the maxilla), while the Y-axis is perpendicular to the XZ-plane and points dorsally. Indicated on the model drawings beneath the lateral and ventral pictures are: width (w_i), height (h_i) and length (l_i) of the elliptical cylinders that constitute the pipefish's head and body, vectors $\boldsymbol{r}_i$ between CR and the centres of mass of each subdivision, angle β_i between the anterior–posterior axis of the head and $\boldsymbol{r}_i$. The direction of positive angular velocity ω (vector notation $\omega\hat{\boldsymbol{z}}$) is indicated by the dashed arrow. The dashed line separates head and body in the model. More information is given in the text and appendix A.

23.31 mm (distance between the premaxilla and the occipital process). These pipefish will be referred to as the first and second individual, respectively. They were filmed capturing live mysid shrimp held by forceps using a Redlake MotionScope digital video camera (filming at 2000 Hz; shutter 1/4000 s; 160×140 pixels). The field was lit with two 600 W tungsten photo lamps. Nine and ten sequences of the first and second individual were used to determine velocity and acceleration of head rotation, respectively. These sequences only included recordings in which the sagittal plane of the pipefish was approximately perpendicular to the symmetry axis of the camera lens (less than 15°).

Eighteen additional high-speed videos were selected from prey captures of eight bay pipefish that were caught in Elkhorn Slough, an estuarine region of Monterey Bay on the central California coast, USA. The cranial length of these individuals ranged from 20.7 to 35.2 mm. The experimental set-up differed from the one described above by a lower frame rate that was used during the high-speed video recordings (1000 Hz). Live *Artemia salina* were used as prey. Owing to the higher spatial resolution of the digital images

(240×210 pixels), these videos were used to determine the positional variables used in the model (CR, p, ϕ_0; see further) with higher accuracy than could be done based on the 2000 Hz videos.

2.2. Kinematics

The head angle (θ) with respect to the horizontal axis was determined for each of the 19 sequences recorded at 2000 Hz. To do so, four landmarks were digitized on every high-speed video frame using Didge (Alistair Cullum, Creighton University, Omaha, USA): a dorsal and a ventral landmark at the tip of the snout (landmarks 1–2), and a dorsal and a ventral landmark posterior of the head (landmarks 3–4), at the level of the opercular opening (figure 2). From the XY coordinates of these points, the angle θ was determined between the line connecting the centres of landmarks 1–2 and 3–4 and the horizontal. Time zero was assigned to one frame before hyoid movement was observed externally. Also, the angle (ϕ_0) between the head and the centreline of the body was determined on the time zero frame (figure 2).

Digitization noise was filtered on the angle (θ) versus time profiles using a zero-phase shift, fourth-order low-pass Butterworth filter with a cut-off frequency of 500 Hz. Angular velocities (ω) and accelerations (α) are respectively calculated by

$$\omega_{(t1+t2)/2} = \frac{(\theta_{t2} - \theta_{t1})}{\Delta t} \tag{2.1}$$

and

$$\alpha_{t2} = \frac{(\omega_{(t2+t3)/2} - \omega_{(t1+t2)/2})}{\Delta t}, \tag{2.2}$$

where Δt is the time step of the videos (0.5 ms), and subscripts denote time-sequential frame numbers.

Since head rotation in *S. leptorhynchus* generated a countermovement of the body (figure 2), the instantaneous centre of rotation of the head will probably be time-dependent (see also de Lussanet & Muller 2007). However, in order to reduce the mathematical complexity of the model, a fixed centre of rotation (CR) was used. To allow an estimate of maximal power requirement, the position of this fixed CR should ideally correspond to the instantaneous CR at the time of maximal power requirement. Because inertial forces probably dominate the dynamics of head rotation in pipefish (de Lussanet & Muller 2007), the force will be roughly proportional to acceleration, and peak power (force×velocity) will be reached near the instant when the product of acceleration and velocity becomes maximal. As peak angular acceleration and velocity of the head of *S. leptorhynchus* occurred on average after 1.0 and 2.0 ms, respectively, and the product of velocity and acceleration peaked at time $t=1.5$ ms, $t=1.5$ ms will probably be the instant of maximum power requirement. The CR at this instant was approximated by finding the anterior–posterior axis of the head for $t=0.0$ and 3.0 ms using two fixed landmarks (e.g. dorsal tip of the snout, eye or opercular), then drawing a line perpendicular to the midpoint of each of these lines. The intersection point of these two perpendicular lines equals CR (figure 2). The latter procedure is only valid if translation can be neglected. This holds true for *S. leptorhynchus*, which approached its prey at speeds lower than 0.07 m s^{-1}, meaning that the total forward translation during the first 3 ms of the feeding event will always be less than 0.2 mm, a negligibly small fraction of the rotational displacement.

2.3. Model

2.3.1. General outline. An inverse dynamic model was used to calculate the power requirement of dorsal rotation of the head in pipefish during feeding. Following the approach of Drost & van den Boogaart (1986), the model divides the head and body of the pipefish into a series of elliptical cylinders scaled to match the height and width of the head measured at specific positions on a lateral and ventral view photograph (figure 3). Twenty elliptical cylinder sections were used to characterize the head between the upper jaw and the posteriormost point on the operculum. Each section is indicated by an index i (1–20 from the origin to the snout tip). The head was assumed to act as a rigid body during its acceleration phase, since lateral expansion of the snout, thought to be the primary generator of suction in pipefish, does not start until close to the end of dorsal rotation of the head (de Lussanet & Muller 2007).

In the following outline of the model, bold symbols represent vectors. Unit vectors in the X, Y and Z directions were represented by $\hat{\boldsymbol{x}}$, $\hat{\boldsymbol{y}}$ and $\hat{\boldsymbol{z}}$, respectively (figure 3). A unit vector perpendicular to the surface of the elliptical cylinder and directed towards the direction of motion in the midsagittal plane (XY) was named $\hat{\boldsymbol{s}}$ (figure 3). The pipefish was assumed to be fully bilaterally symmetric. In accordance with the kinematic data of syngnathid fishes during prey capture, only movement within the XY-plane was considered.

2.3.2. Equation of motion. The following equation of motion for the head-snout rotating around the CR was used:

$$I\alpha\hat{\boldsymbol{z}} = \boldsymbol{M}_{\mathrm{m}} + \boldsymbol{M}_{\mathrm{d}} + \boldsymbol{M}_{\mathrm{a}}, \tag{2.3}$$

where I is the moment of inertia of the head and snout; $\alpha\hat{\boldsymbol{z}}$ the angular acceleration; $\boldsymbol{M}_{\mathrm{m}}$ is the moment produced by the muscles involved in rotation of the head; $\boldsymbol{M}_{\mathrm{d}}$ is the moment as a result of hydrodynamic drag; and $\boldsymbol{M}_{\mathrm{a}}$ is an additional inertial term due to the resistance of the surrounding water to acceleration (added mass or acceleration reaction). An equal density was assumed for head and body tissues as well as for the surrounding water (1023 kg m^{-3}). Consequently, gravitational force and hydrostatic lift counter each other, and therefore are not considered further.

2.3.3. Moment of inertia. The total moment of inertia of the head is the sum of the moments of inertia of the 20 elliptical cylinders. The moment of inertia of a given elliptical cylinder i rotating around its centre of mass (axis parallel to the Z-axis) is

$$I_i = m_i\left(\frac{h_i^2}{16} + \frac{l_i^2}{12}\right), \tag{2.4}$$

with mass $m_i=(1/4)\rho\pi w_i h_i l_i$. According to the parallel axis theorem for moments of inertia, the total moment of inertia of the head rotating about an axis through CR parallel to the *Z*-axis becomes

$$I=\sum_{i=1}^{20} m_i\left(\frac{h_i^2}{16}+\frac{l_i^2}{12}+r_i^2\right), \tag{2.5}$$

where r_i is the distance from CR to the centre of mass of the elliptical cylinder.

2.3.4. Drag. The total moment of force due to hydrodynamic drag equals the summation of the moments for the individual elliptical cylinders given by

$$\boldsymbol{M}_{\mathrm{d}}=\sum_{i=1}^{20}(\boldsymbol{r}_i\times\boldsymbol{F}_{\mathrm{d},i}). \tag{2.6}$$

Since for a given angular velocity $\boldsymbol{\omega}=\omega\hat{\boldsymbol{z}}$, the linear velocity of the centre of mass of each element $\boldsymbol{v}_i=\boldsymbol{\omega}\times\boldsymbol{r}_i$ will be directed opposite to the incident flow relative to the moving body

$$\boldsymbol{F}_{\mathrm{d},i}=-\frac{1}{2}C_{\mathrm{d}}\rho A_{p,i}|\boldsymbol{v}_i|\boldsymbol{v}_i, \tag{2.7}$$

where the drag coefficient C_{d} is a function of size, shape, velocity and surface roughness (smooth surfaces are assumed in the model calculations) of the object. The C_{d} for a long elliptical cylinder in laminar flow ($Re<2\times10^5$) is approximately 1.0 if the aspect ratio in the *YZ*-plane is circular ($h_i=w_i$), but decreases when ratio h_i/w_i becomes higher. The relationship between drag coefficient of long elliptical cylinders and their aspect ratios presented by Blevins (1984) was approximated by

$$C_{\mathrm{d}}=1.0355(h_i/w_i)^{-0.9896}\ (0.75<h_i/w_i<6). \tag{2.8}$$

This drag coefficient is also a function of Reynolds number (Re): for external flow over smooth cylinders, C_{d} will drop off considerably in the transition to turbulent flow regimes ($Re>2\times10^5$; Hoerner 1965; Schlichting 1979). However, this critical Re is not likely to be reached during head rotation in pipefish, since Re will maximally be about 7×10^4, representing a case where a velocity of 3.5 m s^{-1} (higher than the measured peak velocities of the mouth) and a characteristic length of 20 mm (approximate head length) were used to calculate Re. It was therefore assumed that the model operates in the flow regime where C_d can be roughly considered independent of Re ($400<Re<2\times10^5$).

The surface area of each elliptical cylinder projected onto the plane perpendicular to the direction of motion (tangential to the circular path at a given instant) is given by

$$A_{p,i}=l_i w_i|\cos\beta_i|, \tag{2.9}$$

where β_i is the angle between the anterior–posterior axis of the head and the line between the CR and the centre of mass of the elliptical cylinder. By using the projected area of the external surface area of an elliptical cylinder, drag force decreases sinusoidally with the angle of attack of the surface moving through the water, which is in accordance with the experimental measurements (Munshi *et al.* 1999; Bixler & Riewald 2002).

2.3.5. Added mass. The total linear acceleration of each section $\boldsymbol{a}_i$ results from both angular and centripetal acceleration, and is given by

$$\boldsymbol{a}_i=\alpha\hat{\boldsymbol{z}}\times\boldsymbol{r}_i-\boldsymbol{r}_i\omega^2, \tag{2.10}$$

where α and ω are the instantaneous angular acceleration and velocity of the head, respectively. Since added mass for acceleration along the axis of rotation of an infinitely long cylinder equals 0 (assuming potential flow conditions), the added mass force $\boldsymbol{F}_{\mathrm{a},i}$ acts normal to the surface of the pipefish and can be calculated by

$$\boldsymbol{F}_{\mathrm{a},i}=-(\boldsymbol{a}_i\cdot\hat{\boldsymbol{s}})\hat{\boldsymbol{s}}C_{\mathrm{a}}m_i, \tag{2.11}$$

where C_{a} is the added mass coefficient and m_i the mass of the elliptical cylinder. From equations (2.10) and (2.11), we find that

$$\begin{aligned}\boldsymbol{a}_i\cdot\hat{\boldsymbol{s}}&=\alpha\hat{\boldsymbol{s}}\cdot(\hat{\boldsymbol{z}}\times\boldsymbol{r}_i)-\omega^2\hat{\boldsymbol{s}}\cdot\boldsymbol{r}_i\\&=\alpha r_i\cos\beta_i+\omega^2 r_i\sin\beta_i.\end{aligned} \tag{2.12}$$

Next, the moment that is generated is

$$\begin{aligned}\boldsymbol{M}_{\mathrm{a},i}&=\boldsymbol{r}_i\times\boldsymbol{F}_{\mathrm{a},i}\\&=(\alpha r_i\cos\beta_i+\omega^2 r_i\sin\beta_i)C_{\mathrm{a}}m_i(\hat{\boldsymbol{s}}\times\boldsymbol{r}_i).\end{aligned} \tag{2.13}$$

Since $\hat{\boldsymbol{s}}\times\boldsymbol{r}_i=-r_i\cos\beta_i\hat{\boldsymbol{z}}$, the total moment caused by added mass can be calculated by

$$\begin{aligned}M_{\mathrm{a}}=-\sum_{i=1}^{20}C_{\mathrm{a}}m_i(&\alpha r_i^2\cos^2\beta_i\\&+\omega^2 r_i^2\sin\beta_i\cos\beta_i).\end{aligned} \tag{2.14}$$

During the acceleration phase of head rotation, M_{a} resists movement, which explains the negative sign in the above equation. C_{a} differs for each of the elliptical cylinders as a function of aspect ratio h_i/w_i. The added mass coefficients of elliptical cylinders with a range of different aspect ratios are given by Daniel (1984). The relationship presented in his study was approximated by

$$C_{\mathrm{a}}=2.1438\exp(-0.7841\ h_i/w_i)\ (0.75<h_i/w_i<3). \tag{2.15}$$

Near the opercular region the aspect ratio is approximately 1, resulting in a C_{a} of 1.0. In contrast, aspect ratios of about 2.5 were reached near the snout tip, which resulted in a considerably lower C_{a} of 0.4 (Daniel 1984).

2.3.6. Body movement. Because not only the head was moved during prey capture but also the body, the centre of rotation of the head during prey capture was located dorso-caudally of the eye (figure 3). Initially, the anterior part of the body was depressed and slightly drawn forward. Later, this movement of the body continued as a wave running down the body in *S. leptorhynchus*. To include the movement of the anterior part of the body in the inverse dynamic

calculations, the distance from the posterior edge of the opercular to a landmark on the body (p) was determined, where movement could be considered negligible during the initial phase of head rotation (figure 2). To perform the model calculations, the anterior part of the body was divided into a series of 20 elliptical cylinders, and indicated by index i (-1 to -20 from the origin to p). To obtain an approximation of the power that goes into this countermovement of the body, each of these elements is assumed to follow the displacement of the origin (0, 0, 0) by a translation multiplied by a factor c. Factor c decreases linearly with the distance from the origin (where $c_i=1$) to point p (where $c_i=0$) so that total displacement, velocity and acceleration decrease gradually from the pectoral region towards p.

The following equation of motion was used as an approximation for the dynamics of the countermovement of a given body section i:

$$m_i(c_i\alpha\hat{\boldsymbol{z}}\times\boldsymbol{r}_0) = \boldsymbol{F}_{\text{m-body},i}+\boldsymbol{F}_{\text{d-body},i}+\boldsymbol{F}_{\text{a-body},i}, \tag{2.16}$$

where vector $\alpha\hat{\boldsymbol{z}}\times\boldsymbol{r}_0$ is the vector of angular acceleration of the landmark on the pipefish corresponding to the origin of the coordinate system shown in figure 3. The forces on the right-hand side of the equation are due to, from left to right, muscle–tendon activity, drag and added mass, respectively. First, we need to define ε, the angle between the unit vector perpendicular to the surface ($\hat{\boldsymbol{s}}$) and the velocity vector ($\boldsymbol{v_0}$) or acceleration vector ($\alpha\hat{\boldsymbol{z}}\times\boldsymbol{r}_0$). This time-dependent angle is given by

$$\varepsilon=\pi-\beta_0+\theta-\theta_0-\phi_0, \tag{2.17}$$

where β_0 is the angle between the X-axis and the line connecting CR to origin point of the model posterior of the head; θ_0 is the head-to body angle at time zero; $\theta-\theta_0$ is the angle rotated by the head since the start of the strike at the prey; and ϕ_0 the angle between the X-axis and the longitudinal axis of the body (figures 2 and 3).

The drag force on the body was calculated by

$$\boldsymbol{F}_{\text{d-body},i}=-\frac{1}{2}C_{\text{d}}\rho l_i w_i\cos\varepsilon|c_i\boldsymbol{v}_0|c_i\boldsymbol{v}_0, \tag{2.18}$$

where $c_i\boldsymbol{v_0}$ is the linear velocity of a given section of the body and $l_i w_i\cos\varepsilon$ the area projected onto the plane perpendicular to the direction of motion. Similar to equation (2.11), the force due to added mass was calculated by

$$\boldsymbol{F}_{\boldsymbol{a\text{-}body,i}}=-[(c_i\alpha\hat{\boldsymbol{z}}\times\boldsymbol{r}_0)\cdot\hat{\boldsymbol{s}}]\hat{\boldsymbol{s}}C_a m_i. \tag{2.19}$$

By taking the scalar product of velocity $c_i\boldsymbol{v_0}$ and both sides of equation (2.16), after some rearrangement we find that

$$c_i\boldsymbol{v}_0\cdot\boldsymbol{F}_{\text{m-body},i} = c_i\boldsymbol{v}_0\cdot m_i(c_i\alpha\hat{\boldsymbol{z}}\times\boldsymbol{r}_0)-c_i\boldsymbol{v}_0\cdot\boldsymbol{F}_{\text{d-body},i} - c_i\boldsymbol{v}_0\cdot\boldsymbol{F}_{\text{a-body},i}. \tag{2.20}$$

Since power (P) equals the product of force and velocity, $\boldsymbol{v}_0\cdot\hat{\boldsymbol{s}}=\boldsymbol{v}_0\cos\varepsilon$ and $v_0=\omega\, r_0$, after substitution of equations (2.19) and (2.20) this equation becomes

$$P_{\text{m-body},i}=\omega m_i\alpha r_0^2c_i^2+\frac{1}{2}C_{\text{d}}\rho l_i w_i(c_i\omega r_0)^3\cos\varepsilon + C_{\text{a}}m_i c_i^2\omega\alpha r_0^2\cos^2\varepsilon. \tag{2.21}$$

2.3.7. Power requirement. Finally, the total instantaneous power required for the rotation of the head and the consequent movement of the anterior part of the body observed during prey capture was calculated by

$$P_{\text{m}}=\omega M_{\text{m}}+\sum_{i=1}^{20}P_{\text{m-body},i}, \tag{2.22}$$

where M_{m} can be obtained using equation (2.3), and $P_{\text{m-body},i}$ from equation (2.21).

2.3.8. Rotational forces. Since the head of the pipefish is rotating as well as translating, there is the potential for 'rotational forces' beyond the hydrodynamic forces we have described (Kramer 1932; Sane & Dickinson 2002). However, such rotational forces are typically of minor importance for foils rotating about an axis that is perpendicular to the long axis of the foil (a rotor), unless either the induced flow velocity or the advance ratio (the ratio of the freestream velocity to the velocity at the tip of the foil) is unusually large (Leishman 2006). Since the lift coefficient of the pipefish head is nearly 0 (as a result of left–right symmetry) induced flow is expected to be small, and the maximum advance ratio that was observed during the feeding manoeuvre was less than 0.1. Consequently, any rotational contribution to the force on the pipefish head is expected to be small and we will assume it to be 0.

2.4. Electromyography

EMG of the epaxial muscle was performed simultaneously with high-speed video recordings (2000 Hz). The epaxial muscle was chosen because it is the largest muscle used for powering neurocranial elevation and expansion of the mouth cavity. In addition, both left and right portions of the epaxials insert onto the neurocranium via a relatively large tendon (figure 1). Consequently, if elastic energy storage and release do occur, it is expected to be found in the epaxial muscles.

Prior to implantation of the electrodes, the animals were anaesthetized with MS 222 (tricaine methanesulfonate, Argent Finquel). A surgical twist drill was used to create a very small hole (diameter less than 1 mm) into the bony plates that cover the epaxial muscles. Next, a PrecisionGlide 26G1/2 hypodermic needle (BD, Franklin Lakes, USA) was used to insert a red nylon coated, stainless steel bipolar electrode (California Fine Wire Company, Grover Beach, USA) into the left side of the epaxial muscle, approximately half a head length posterior to the pectoral girdle.

The electrode was connected to a differential AC amplifier Model 1700 (A-M Systems, Inc., Sequim, USA; bandpass filter 10–1000 Hz) and recorded with a National Instruments DAQPad-6020E (National Instruments Corporation, Austin, USA). EMG

measurements were pre-trigger captured using MATLAB v. 7.1 (The MathWorks Inc., Natick, USA) and sampled at a rate of 10 kHz.

In order to investigate whether there are characteristic features of the EMG intensity in time–frequency space, a wavelet analysis was performed on the measured EMG signals (Torrence & Compo 1998). This has the advantage over the Fourier transform in that the wavelet transform allows not only characteristic frequencies of periodicities to be determined, but also the localization on the time axis to be detected (Ippolitov *et al.* 2002). The analysis yields an intensity that approximates closely the power of the EMG signal (Wakeling *et al.* 2001). Morlet wavelets were used following the procedures outlined by Torrence & Compo (1998). Wavelet software was provided by C. Torrence and G. Compo, and is available at URL: http://paos.colorado.edu/research/wavelets/.

In total, 39 suction feeding sequences were analysed. Some of these were initial strikes at the prey (13 and 12 sequences for the first and second individual, respectively), while in others the prey was held between the oral jaws and suction was used to transport the prey through the tubular snout (5 and 9 sequences). The differences between both types of suction in the duration of pre-strike activation were tested with two-way ANOVA (suction type, fixed effect; individual, random effect) using STATISTICA 5.0 (Statsoft, Tulsa, USA).

A correlation between three EMG variables (onset time, peak amplitude and total volume underneath the surface of the wavelet-transformed EMG) and peak instantaneous power output of head rotation and body movement calculated by the model was tested using a linear, least-squares correlation analysis. For the latter two of these three EMG variables, this analysis could only be performed on one individual ($N=9$) due to EMG amplitude decreasing gradually in course of the recording session for the other pipefish. The significance level of $p=0.05$ was used.

2.5. Morphology

Two *S. leptorhynchus* individuals (23.77 and 25.47 mm cranial length) were sacrificed by overdose of the MS222, and dissected under a dissection scope coupled to a digital camera. The left and right epaxials and hypaxials were removed and weighed (± 0.0001 g). Since both epaxials and hypaxials could be responsible for dorsal rotation of the head in pipefish, the mass of both the muscles was used to calculate muscle-mass-specific power requirement (i.e. total power requirement divided by muscle mass). In order to reach a conservative estimate of muscle-mass-specific power requirement, the muscle mass from the individual with largest muscle mass was used. The epaxials and hypaxials of this *S. leptorhynchus* of 25.47 mm cranial length weighed 32.2 and 16.5 mg, respectively. Isometric growth was assumed to convert morphological data between individuals of different body sizes. As the range of body sizes of the animals used to study kinematics, EMG and morphology was relatively narrow, potential deviations from isometric scaling in our data was assumed to be negligibly small, and would thus not influence the presented data.

3. RESULTS

3.1. Kinematics

A stereotypical pattern of dorsal head rotation was observed for two *S. leptorhynchus* individuals during prey capture (figure 4). Especially during the first 3 ms after the start of the hyoid rotation, relatively small standard deviations of head angle versus time profiles are shown for the different feeding sequences within each individual. When comparing the mean kinematic profiles between both individuals, the time of peak velocity (2.0 ms) and peak acceleration (1.0 ms) are identical (figure 4). In addition, the data from the individual sequences did not differ in more than one video frame (± 0.5 ms) from this mean time of peak velocity and peak acceleration.

The position of the centre of rotation of the head (CR) lies slightly dorso-caudally of the eye (figure 3; table 1). Mean values for the head-to-body angle (ϕ_0) and the approximate anteriormost stationary point on the body during the initial phase of prey capture (p) are presented in table 1. Because the mean values of peak velocity and peak acceleration after pooling the data from both individuals (table 1) was qualitatively a better match to the mean kinematic profile of the first individual (figure 4; upper graphs), this kinematic profile (angle, velocity and acceleration) was used as input in the model.

3.2. Dynamics

A peak instantaneous muscle-mass-specific power requirement of 5795 W kg^{-1} was calculated by the model (figure 5). This value includes power that is required to rotate the head (2641 W kg^{-1}) and power that goes into the anteroventral movement of the anterior part of the body (3154 W kg^{-1}). This power is more than five times the highest peak instantaneous contractile power output measured *in vitro* for vertebrate muscle: 1121 W kg^{-1} for the pectoralis of quail (Askew & Marsh 2001). Peak power requirement is reached 1.5 ms after the start of the prey capture event.

When movement of head and body is considered together, the highest proportion of the power produced by the muscle goes directly into the acceleration of the mass of the pipefish (inertial forces dominate). At the instant of maximum power requirement, 51% of the total power is required to overcome inertia of the head and body. The added mass of the surrounding water accounts for 40% of the total power required from the muscles. Steady-state drag forces are the least important, requiring 9% of power of prey capture in *S. leptorhynchus*.

However, the relative importance of each of these forces differs between the rotation of the head and the countermovement of the body (figure 5*b*,*c*). Since the head is considerably more streamlined than the body with respect to movement in the dorsoventral direction, the forces resulting from the effect of added mass of the surrounding water are considerably less important than those needed to accelerate the mass of the head itself; added mass results in only 55% of 'inertial force' of the rotation of the head (figure 5*b*), but is approximately equal to the latter for the body movement of the pipefish (figure 5*c*).

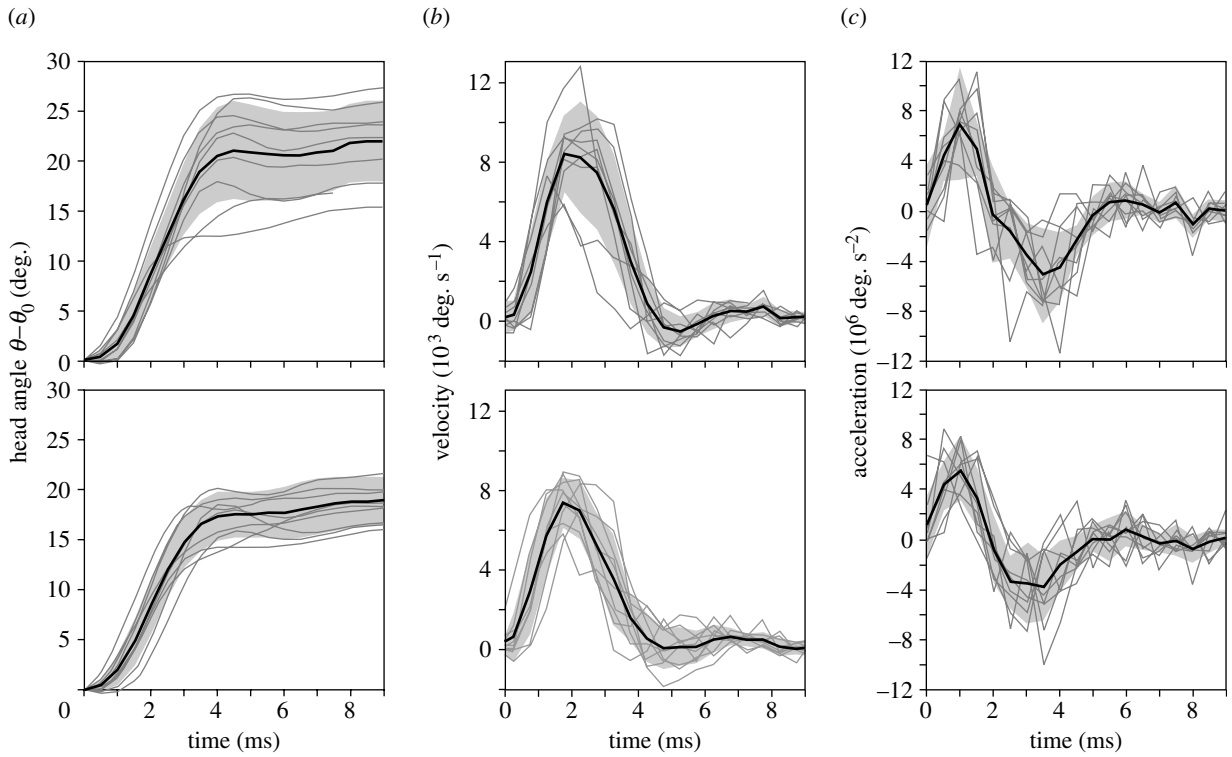

Figure 4. Mean kinematic profiles for angle (*a*), velocity (*b*) and acceleration (*c*) of the head during prey capture from two individuals (upper and lower graphs; $N=9$ and 10). The grey zone indicates mean $\pm$ s.d. The grey lines represent the data from individual feeding sequences.

3.3. Epaxial muscle activity

Activation of the epaxial muscle always started at least 105 ms before the rotation of the head and hyoid. The average onset time was -209 ± 74 and -258 ± 112 ms (mean $\pm$ s.d.) for the first and second individual, respectively. *S. leptorhynchus* showed a significantly longer period of epaxial muscle activity for initial prey captures (271 ± 21 ms; mean $\pm$ standard error) when compared with sequences where the prey was transported from the mouth into the mouth cavity (172 ± 9 ms; $F_{1,35}=13.9$; $p=0.0007$). Also, a considerably larger variation in onset times was observed for initial prey captures (105 ms s.d.) when compared with prey transport sequences (33 ms s.d.). Note, however, that no differences could be discerned for these two types of feeding sequences between the duration of complete head rotations (5.1 ± 0.3 ms for initial strikes; 4.9 ± 0.4 ms for prey transports; $F_{1,35}=0.58$, $p=0.45$), the total angle rotated by the head ($19.2\pm1.1°$ and $16.2\pm3.2°$; $F_{1.15}=28.4$, $p=0.12$, respectively), the peak velocity (8.3 ± 0.3 and $8.5\pm0.3\times10^{3\circ}\,s^{-1}$; $F_{1,15}=0.009$, $p=0.94$, respectively) and peak acceleration of the head (7.5 ± 0.5 and $8.1\pm0.9\times10^{6\circ}\,s^{-2}$; $F_{1,15}=11.3$, $p=0.18$, respectively).

Following onset, EMG amplitude increased gradually and reached a maximum near 49 ± 22 ms (mean $\pm$ s.d.) prior to the start of the strike at the prey (figure 6). Around this time, the wavelet analyses typically indicate a short, final burst lasting approximately 15 ms where a high-power, high-frequency activation of the epaxial muscle occurs (figure 6). After this, the epaxial activation decreases steeply to near-zero values (i.e. the noise level of the EMG signal) around 10 ± 6 ms before the prey capture motion starts. The activation intensity recovers to a sub-maximal level during and after the head rotation phase (figure 6).

Table 1. Mean kinematic data of prey capture in *S. leptorhynchus*. (CL, cranial lengths; °, degrees. Figure 2 and appendix A define p and ϕ_0. The XY-reference frame is illustrated in figure 3.)

	mean	s.d.	N
X-coordinate of centre of rotation (CL)	0.325	0.052	37
Y-coordinate of centre of rotation (CL)	0.083	0.044	37
p (CL)	0.74	0.15	52
ϕ_0 (°)	12.9	5.0	37
total head rotation (°)	20.1	4.0	19
peak velocity of head rotation ($10^{3\circ}\,s^{-1}$)	8.36	1.64	19
peak acceleration of head rotation ($10^{6\circ}\,s^{-2}$)	7.62	1.85	19

Peak EMG amplitude showed a significant, positive correlation with peak instantaneous power of head rotation ($R^2=0.56$; $F_{1,8}=8.8$, $p=0.021$). However, no significant correlation was observed between the duration from the onset of activation of the epaxial muscle and the start of head rotation (figure 7; $R^2=0.026$; $F_{1,18}=0.45$, $p=0.51$) and peak power requirement calculated by the model, or between the total volume underneath the wavelet-transformed EMG (i.e. a measure of total activation intensity; $R^2=0.19$; $F_{1,8}=1.7$, $p=0.24$) and this peak power requirement.

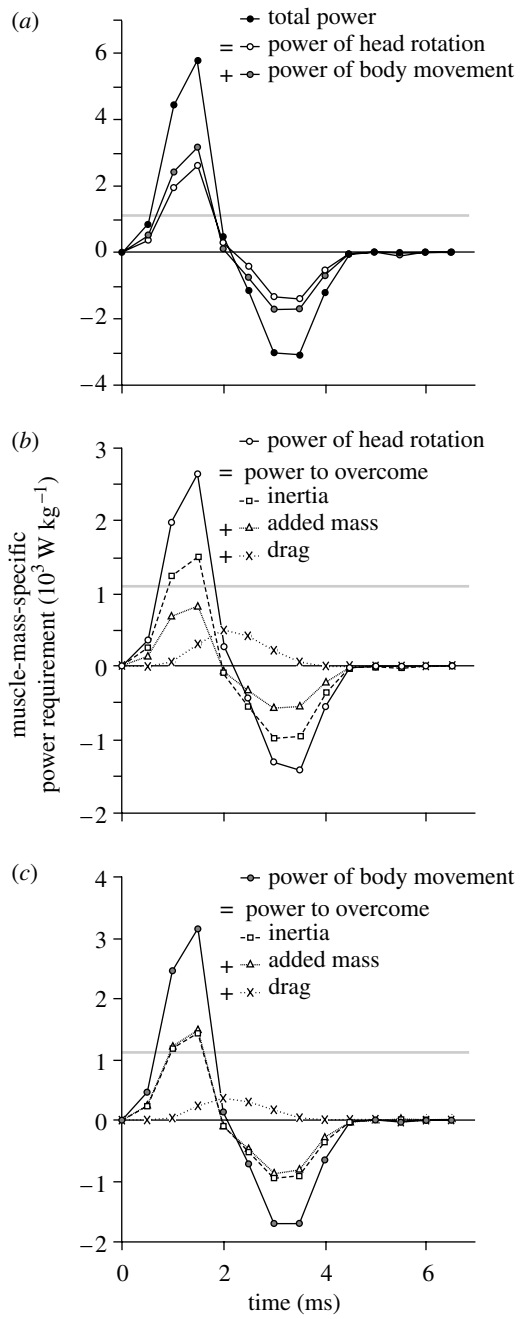

Figure 5. Instantaneous power requirement during prey capture in *S. leptorhynchus* as calculated by inverse dynamic modelling. The total power that needs to be generated by the epaxial and hypaxial muscle–tendon complexes to cause the observed feeding manoeuvre equals the sum of the powers needed to rotate the head and translate the anterior part of the body (*a*). The grey line at 1121 W kg^{-1} indicates the highest peak instantaneous contractile power output measured for vertebrate muscle (Askew & Marsh 2001). Power requirement values exceeding this line demonstrate the use of an elastic power enhancement mechanism. Graph (*b*) shows that overcoming the head's inertia is the dominant factor in the dynamics of head rotation, followed by the effect of added mass and steady-state drag. The dynamics of the countermovement of the body are dominated by the body's inertia as well as the effect of added mass of the surrounding water (*c*). Drag is less important in the latter case. The negative powers calculated in the deceleration phase (after time = 2 ms) of head rotation in (*b*) imply that energy can be restored in elastic structures of the feeding system (for example the protractor hyoidei tendons) or used to generate suction.

4. DISCUSSION

The results of the present study provide the first experimental evidence for the presence of a catapult-like mechanism of prey capture in syngnathid fishes, as proposed by Muller (1987). The power requirement of 5795 W kg^{-1} calculated by the inverse dynamic model described earlier probably requires that the bay pipefish (*S. leptorhynchus*) uses a mechanism of elastic power enhancement. Elastic elements are present in the form of the tendons of the epaxial and hypaxial muscles (figure 1), of which the primary function is to rotate the head and snout towards the prey and to retract the hyoid. The larger of these two muscles, the epaxial muscle, is activated for a relatively long duration (between 104 and 586 ms) before any movement of the feeding apparatus can be observed externally (figure 6). This implies that the epaxial tendons will be strained prior to the strike, enabling sudden elastic recoil to cause accelerations beyond the capacity of normal cross-bridge-driven contraction of muscle.

It is therefore not surprising that the activation patterns of the epaxial muscle prior to and during prey capture in the bay pipefish (figure 6) show remarkable similarity with those recorded for other vertebrates that use elastic power amplification mechanisms during feeding. The tongue projector muscles in chameleons (Wainwright & Bennet 1992) and salamanders (Deban *et al.* 2007), as well as the muscles causing ballistic mouth opening in toads (Lappin *et al.* 2006) also show a gradually increasing EMG intensity, followed by a deactivation a few milliseconds before the start of the explosive motion. An explanation for this deactivation is given by Lou *et al.* (1999), who showed that energy stored in the series elastic components of dogfish axial muscle could be recovered completely as external work when the muscle shortened during relaxation, whereas only 80% of the energy was recovered if the muscle remained stimulated during shortening. The offset of activation of the epaxial muscles of the pipefish (acting in series with the pre-stressed, long epaxial tendons) prior to shortening may therefore save a certain amount of metabolic energy, of which probably only a negligibly small fraction could be converted into work for rotating the head towards prey in case of a prolonged epaxial activation.

Although muscle activity patterns were only recorded for the epaxial muscle, the hypaxial muscle probably shows a similar pattern of activation. If not, force would be exerted by the epaxials on the dorsal side of the vertebral column without being countered by force from the hypaxials originating ventrally of the vertebral column (see figure 1). Since the body can easily be flexed in the dorsoventral direction, this situation would inevitably result in dorsal bending of the body. Our high-speed videos clearly show that this is not the case. Thus, we expect the onset of activation of the hypaxials to be approximately simultaneous with that of the epaxial muscles.

It should be noted that the shortest durations of epaxial muscle activation only occurred during suction-transport sequences where the prey was already caught between the jaws. When prey were caught from a distance, the phase where epaxial tendon strain is

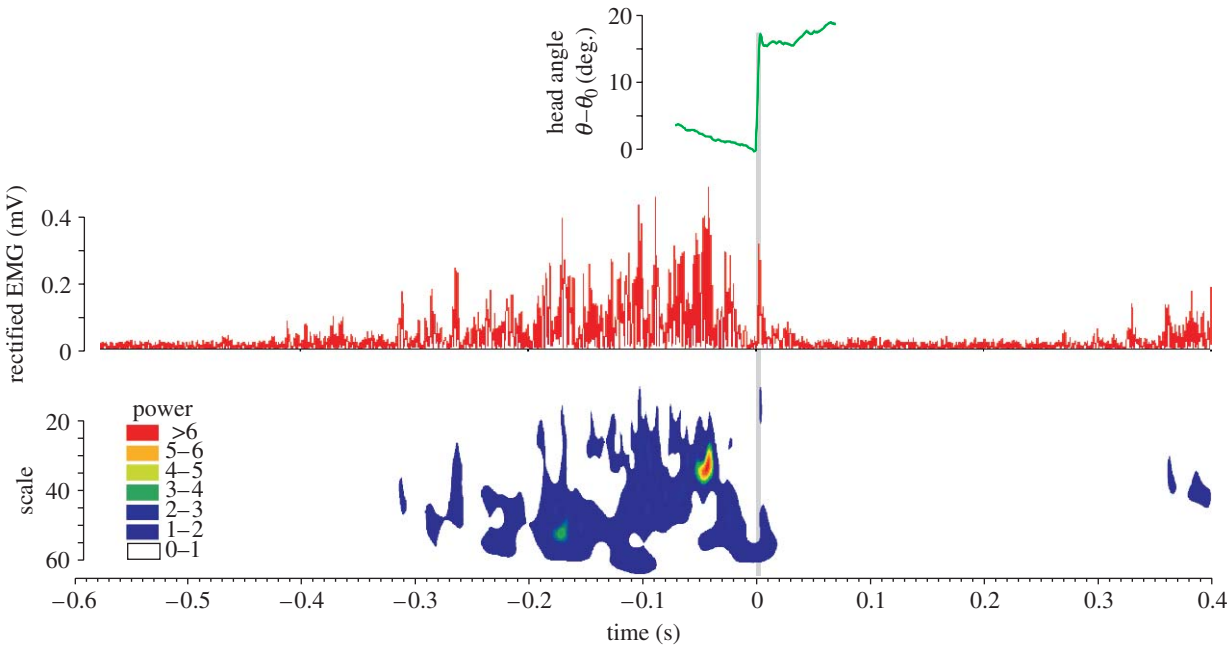

Figure 6. Representative example of an EMG of the epaxial muscle during prey capture in *S. leptorhynchus*. The graphs show head rotation kinematics (green), rectified EMG signal (red) and a contour plot resulting from the Morlet wavelet analysis. The phase of fast dorsal rotation of the head is indicated by the grey bar (time 0 until 0.0055 s). Note that the scale axis of the wavelet graph is inversely related to frequency so that regions on the graph further away from the time axis represent higher EMG frequency. Colour codes indicate EMG power.

increased by muscle contraction lasted longer, and the variability in activation duration increased. Since our data also show that power requirement of head rotation did not decrease significantly with shorter activation times of the epaxial muscles (figure 7), we hypothesize that pipefish are capable of keeping the hypaxial and epaxial tendons under stress for some time, waiting for the moment when the prey is at the right position to initiate the strike. The decision to start the strike may be postponed until the moment around 50 ms before the start of head rotation, where we typically observed a burst of intense epaxial muscle activity (figure 6).

The precise mechanism that triggers the release of the catapult mechanism in syngnathid fishes remains unresolved. We can only infer from the presented results that a chain of coupled elements formed by the neurocranium, suspensorium, interhyals and ceratohyals (see figure 1) does not automatically 'unfold' when force is applied on it by the most powerful muscles in the system (epaxials and hypaxials). Potential trigger muscles include the protractor hyoidei (Muller 1987), as well as any other muscle that may cause an abduction of the hyoid (de Lussanet & Muller 2007).

In conclusion, the present study demonstrates that the rapid rotation of the head and snout towards prey in the bay pipefish *S. leptorhynchus* requires extremely high power and involves a mechanism of storage and release of elastic energy. Energy is stored in the large tendons of the epaxial muscles, and most likely also in the hypaxial muscle tendons. The duration during which these elastic elements are brought under tension is variable, and can potentially be fine-tuned awaiting the best moment to initiate the strike at the prey. Several dynamic aspects of the extremely fast rotation of the head towards the prey, such as muscle activation patterns, acceleration and muscle-mass-specific power requirement, are comparable to other explosive movements such as projectile tongues of chameleons, frogs and salamanders.

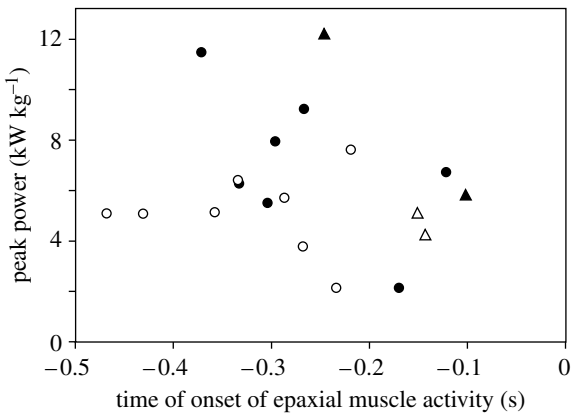

Figure 7. Scatterplot from 19 feeding sequences from 2 individuals (black and white symbols) of *S. leptorhynchus* showing peak instantaneous muscle-mass specific power requirement of head and body movement during feeding versus the time where EMG recordings indicated activation onset of the epaxial muscle (time 0=start of rotation of the head). Circles and triangles indicate initial prey captures and prey transport sequences, respectively. No significant correlations are observed for these data.

All procedures involving animals were approved by the Institutional Animal Care and Use Committee at the University of Washington.

The authors gratefully acknowledge the staff and students at the Friday Harbor Laboratories during the summer of 2006 for their enthusiasm and help during this project. Many thanks to A. P. Summers for giving us the opportunity, and for his assistance during the EMG experiment. Thanks to

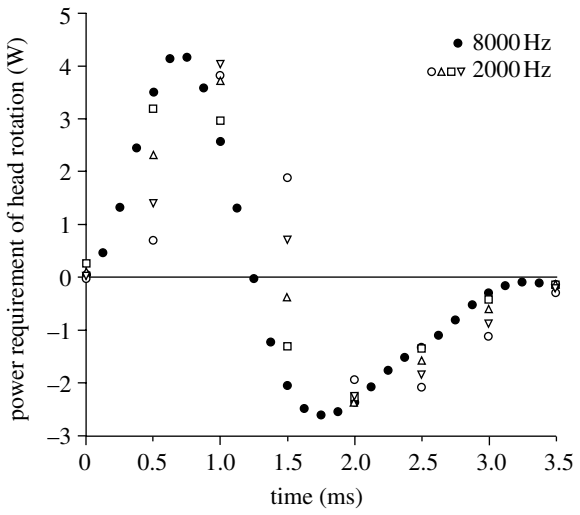

Figure 8. Appendix B instantaneous power requirement of head rotation for a representative prey capture sequence of *Hippocampus reidi* filmed at 8000 frames per second (black circles). The open symbols represent the model output in case the same movie would have been sampled at 2000 frames per second (four possible samplings). Note that peak power calculated by the model using 2000 Hz data is between 77 and 97% of the peak power requirement based on 8000 Hz data. The total positive work tends to be consistently, slightly overestimated due to the reduced sampling frequency of 2000 Hz (103 to 109% when compared with 8000 Hz). The inaccuracy in pinpointing the starting time from 2000 frames per second video generally results in peak power requirements calculated at a couple of tenths of a millisecond later than in reality.

K. D'Août for help with the EMG analysis, and to C. Rinewalt, D. Ardizone, C. Davis, T. Trejo for their assistance in collecting high-speed video. Thanks to G. Roos for providing the data on *Hippocampus reidi*. We wish to thank the four reviewers for their valuable suggestions on how to improve this article. The University of Washington, the University of Antwerp and the Fund for Scientific Research—Flanders (FWO-Vl; grant number G 053907 to P.A.) provided financial support. S.V.W. is a postdoctoral fellow of the FWO-Vl. The equipment used in this study was purchased via NSF grant MRI-0320972 to L.F.G.

APPENDIX A. LIST OF VARIABLES AND CONSTANTS

α	instantaneous angular acceleration of the head
a_i	sectional linear acceleration of the centre of mass
$A_{p,i}$	sectional surface area projected to a plane perpendicular to the direction of motion
β_0	angle between CR, the posteriormost central point of the head, and the head's longitudinal axis
β_i	angle between CR, the centre of mass of head subdivision i, and the head's longitudinal axis
C_a	sectional added mass coefficient
C_d	sectional drag coefficient
c_i	distance between the centre of mass of body section i and point p divided by the distance between the posteriormost point on the longitudinal axis of the head and p
CR	centre of rotation of the head
E	mechanical energy
ε	angle between $\hat{\boldsymbol{s}}$ and $\boldsymbol{v_0}$
ϕ_0	angle between the medial axes of the head and the body
$\boldsymbol{F_{a,i}}$	sectional instantaneous force to account for the effect of added mass
$\boldsymbol{F_{a-body,i}}$	sectional instantaneous force due to added mass of the water
$\boldsymbol{F_{d,i}}$	sectional instantaneous drag force on the head
$\boldsymbol{F_{d-body,i}}$	sectional instantaneous drag force on the body
$\boldsymbol{F_{m-body,i}}$	sectional instantaneous vector of the muscle-tendon force on the body
h_i	height of subdivision I
I	moment of inertia of the head rotating around CR within the sagittal plane
I_i	moment of inertia of a given elliptical cylinder i rotating around the width-axis through its centre of mass
l_i	length of subdivision i along the longitudinal axis
M_a	instantaneous moment due to added mass
M_d	instantaneous moment caused by drag force
m_i	mass of subdivision i
M_m	instantaneous moment generated by muscle–tendon force
p	approximate anteriormost stationary point on the body during the initial phase of prey capture
P	power
P_m	instantaneous power output generated by muscles and tendons
P_{m-body}	instantaneous power generated by muscles and tendons to move the body
$P_{m-body,i}$	P_m for body subdivision i
θ	instantaneous angle of the longitudinal axis of the head with the horizontal axis
θ_0	θ prior to the start of prey capture
ρ	seawater density (1023 kg m^{-3})
Re	Reynolds number
$\boldsymbol{r_0}$	vector from CR to the posteriormost point on the longitudinal axis of the head
$\boldsymbol{r}_i$	vector from CR to the centre of mass of head subdivision I
r_i	length of vector $\boldsymbol{r}_i$
t	time
$\boldsymbol{v_0}$	instantaneous linear velocity vector at the posteriormost point on the longitudinal axis of the head
$\boldsymbol{v}_i$	instantaneous linear velocity vector at head subdivision i
ω	instantaneous angular velocity of head rotation
w_i	width of subdivision i
$\hat{\boldsymbol{x}},\hat{\boldsymbol{y}},\hat{\boldsymbol{z}}$	unit vectors parallel to the axes of the orthogonal coordinate system shown in figure 3

APPENDIX B. EFFECT OF DATA SAMPLING RATE ON MODEL OUTPUT

Sampling data at higher frequency results in a more accurate estimation of velocities and accelerations (Walker 1998). As instantaneous velocities and accelerations are used to calculate the power requirement of

S. leptorhynchus based on kinematic data sampled at 2000 Hz, it is important to know how this sampling rate may have influenced the result of our study. To evaluate this, we additionally performed the model calculations for the sea horse *Hippocampus reidi*, which shows head rotations similar in magnitude and duration when compared with *S. leptorhynchus*, and compared the difference between sampling at 8000 and 2000 Hz (figure 8). This analysis shows that the sampling frequency of the kinematic data used in our study of *S. leptorhynchus* (2000 Hz) tends to underestimate peak instantaneous power requirements by 3 to 23% (figure 8).

REFERENCES

Askew, G. N. & Marsh, R. L. 2001 The mechanical power output of the pectoralis muscle of blue-breasted quail (*Coturnix chinensis*): the *in vivo* length cycle and its implications for muscle performance. *J. Exp. Biol.* **204**, 3587–3600.

Bergert, B. A. & Wainwright, P. C. 1997 Morphology and kinematics of prey capture in the syngnathid fishes *Hippocampus erectus* and *Syngnathus floridae*. *Mar. Biol.* **127**, 563–570. (doi:10.1007/s002270050046)

Bixler, B. & Riewald, S. 2002 Analysis of a swimmer's hand and arm in steady flow conditions using computational fluid dynamics. *J. Biomech.* **35**, 713–717. (doi:10.1016/S0021-9290(01)00246-9)

Blevins, R. D. 1984 *Applied fluid dynamics handbook*. New York, NY: Van Nostrand Reinhold.

Branch, G. M. 1966 Contribution to the functional morphology of fishes. Part III. The feeding mechanism of *Syngnathus acus* Linnaeus. *Zool. Afr.* **2**, 69–89.

Colson, D. J., Patek, S. N., Brainerd, E. L. & Lewis, S. M. 1998 Sound production during feeding in Hippocampus seahorses (Syngnathidae). *Environ. Biol. Fish.* **51**, 221–229. (doi:10.1023/A:1007434714122)

Curtin, N. A., Woledge, R. C. & Aerts, P. 2005 Muscle directly meets the vast power demands in agile lizards. *Proc. R. Soc. B* **272**, 581–584. (doi:10.1098/rspb.2004.2982)

Daniel, T. L. 1984 Unsteady aspects of aquatic locomotion. *Am. Zool.* **24**, 121–134. (doi:10.1093/icb/24.1.121)

De Groot, J. H. & Van Leeuwen, J. L. 2004 Evidence for an elastic projection mechanism in the chameleon tongue. *Proc. R. Soc. B* **271**, 761–770. (doi:10.1098/rspb.2003.2637)

de Lussanet, M. H. E. & Muller, M. 2007 The smaller your mouth, the longer your snout: predicting the snout length of *Syngnathus acus*, *Centriscus scutatus* and other pipette feeders. *J. R. Soc. Interface* **4**, 561–573. (doi:10.1098/rsif.2006.0201)

Deban, S. M., O'Reilly, J. C., Dicke, U. & van Leeuwen, J. L. 2007 Extremely high-power tongue projection in plethodontid salamanders. *J. Exp. Biol.* **210**, 655–667. (doi:10.1242/jeb.02664)

Drost, M. R. & van den Boogaart, J. G. M. 1986 A simple method for measuring the changing volume of small biological objects, illustrated by studies of suction feeding by fish larvae and of shrinkage due to histological fixation. *J. Zool.* **209**, 239–249.

Herrel, A., Meyers, J. J., Aerts, P. & Nishikawa, K. C. 2000 The mechanics of prey prehension in chameleons. *J. Exp. Biol.* **203**, 3255–3263.

Hill, A. V. 1938 The heat of shortening and the dynamic constants of muscle. *Proc. R. Soc. B* **126**, 136–195. (doi:10.1098/rspb.1938.0050)

Hoerner, S. F. 1965 *Fluid-dynamic drag*. Bakersfield, CA: Hoerner Fluid Dynamics.

Ippolitov, I. I., Kabanov, M. V. & Loginov, S. V. 2002 Wavelet analysis of hidden periodicities in some indexes of solar activity. *Russ. Phys. J.* **45**, 1086–1092. (doi:10.1023/A:1023347624436)

Kramer, M. 1932 Die Zunahme des Maximalauftriebes von Tragflugeln bei plotzlicher Anstellwinkelvergrosserung (Boeneffekt). *Z. Flugtech. Motorluftschiff.* **23**, 185–189.

Lappin, A. K., Monroy, J. A., Pilarski, J. Q., Zepnewski, E. D., Pierotti, D. J. & Nishikawa, K. C. 2006 Storage and recovery of elastic potential energy powers ballistic prey capture in toads. *J. Exp. Biol.* **209**, 2535–2553. (doi:10.1242/jeb.02276)

Leishman, J. 2006 *Principles of helicopter aerodynamics*. Cambridge, UK; New York, NY: Cambridge University Press.

Lou, F., Curtin, N. A. & Woledge, R. C. 1999 Elastic energy storage and release in white muscle from dogfish *Scyliorhinus canicula*. *J. Exp. Biol.* **202**, 135–142.

Marsh, R. L. & John-Alder, H. B. 1994 Jumping performance of hylid frogs measured with high-speed cine film. *J. Exp. Biol.* **188**, 131–141.

Muller, M. 1987 Optimization principles applied to the mechanism of neurocranium levation and mouth bottom depression in bony fishes (Halecostomi). *J. Theor. Biol.* **126**, 343–368. (doi:10.1016/0022-5193(82)90287-9)

Muller, M. 1989 A quantitative theory of expected volume changes of the mouth during feeding in teleost fishes. *J. Zool.* **217**, 639–662.

Munshi, S. R., Modi, V. J. & Yokomizo, T. 1999 Fluid dynamics of flat plates and rectangular prisms in the presence of moving surface boundary-layer control. *J. Wind Eng. Ind. Aerod.* **79**, 37–60. (doi:10.1016/S0167-6105(97)00294-8)

Sane, S. P. & Dickinson, M. H. 2002 The aerodynamic effects of wing rotation and a revised quasi-steady model of flapping flight. *J. Exp. Biol.* **205**, 1087–1096.

Schlichting, H. 1979 *Boundary layer theory*, 7th edn. New York, NY: McGraw-Hill.

Stone, M. H., Sanborn, K., O'Bryant, H. S., Hartman, M., Stone, M. E., Proulx, C., Ward, B. & Hruby, J. 2003 Maximum strength–power–performance relationships in collegiate throwers. *J. Strength Cond. Res.* **17**, 739–745. (doi:10.1519/1533-4287(2003)017<0739:MSRICT>2.0.CO;2)

Torrence, C. & Compo, G. P. 1998 A practical guide to wavelet analysis. *Bull. Am. Meteor. Soc.* **79**, 61–78. (doi:10.1175/1520-0477(1998)079<0061:APGTWA>2.0.CO;2)

Vogel, S. 2005 Living in a physical world. III. Getting up to speed. *J. Biosci.* **30**, 303–312.

Wainwright, P. C. & Bennet, A. F. 1992 The mechanism of tongue projection in chameleons. I. Electromyographic tests of functional hypotheses. *J. Exp. Biol.* **168**, 1–21.

Wakeling, J. M. & Johnston, I. A. 1998 Muscle power output limits fast-start performance in fish. *J. Exp. Biol.* **201**, 1505–1526.

Wakeling, J. M., Pascual, S. A., Nigg, B. M. & von Tscharner, V. 2001 Surface EMG shows distinct populations of muscle activity when measured during sustained sub-maximal exercise. *Eur. J. Appl. Physiol.* **86**, 40–47. (doi:10.0007/s004210100508)

Walker, J. A. 1998 Estimating velocities and accelerations of animal locomotion: a simulation experiment comparing numerical differentiation algorithms. *J. Exp. Biol.* **201**, 981–995.